Applied Catalysis B: Environmental 90 (2009) 255–261

Contents lists available at ScienceDirect

Applied Catalysis B: Environmental

journal homepage: www.elsevier.com/locate/apcatb

Enhanced photocatalytic activity of rutile TiO_2 prepared by anodic oxidation in a high concentration sulfuric acid electrolyte

N. Masahashi [a,*], Y. Mizukoshi [a], S. Semboshi [b], N. Ohtsu [c]

[a] Institute for Materials Research, Tohoku University, 2-1-1 Katahira, Aoba-ku, Sendai, Miyagi 980-8577, Japan
[b] Osaka Prefecture University, 1-1 Gakuen-cho, Sakai, Osaka 599-8531, Japan
[c] Kitami Institute of Technology, 165 Koen-cho, Kitami, Hokkaido 090-8507, Japan

ARTICLE INFO

Article history:
Received 5 December 2008
Received in revised form 12 February 2009
Accepted 5 March 2009
Available online 19 March 2009

Keywords:
Photocatalysis
Anodic oxidation
Titanium oxide
Crystallinity
Surface area

ABSTRACT

The photocatalytic characteristics of TiO_2 prepared by anodic oxidation in an electrolyte with a high concentration of sulfuric acid were investigated, focusing on the crystallinity and microstructure of the oxide. The predominant phase in the anodic oxide changes from anatase to rutile with the sulfuric acid concentration; the change appears when this concentration is 0.4 M. Nanosized pores appear in the oxide when the concentration of sulfuric acid is greater than 0.1 M, and the surface area increases with the sulfuric acid concentration. Structural analysis revealed that the inhomogeneous lattice strain in both anatase and rutile is reduced to almost zero, implying that the oxide contains a small number of recombination sites; as a result, the probability of the extinction of the photogenerated charges is low. The methylene blue (MB) bleaching test shows that the photocatalytic activity improves as the concentration of sulfuric acid increases and that the characteristics of rutile are better than those of anatase. It is concluded that rutile-structured TiO_2 exhibits the best photocatalytic activity among the investigated oxides, due to its high crystallinity and porous microstructure.

1. Introduction

TiO_2 has attracted considerable interest due to its high photocatalytic activity and self-cleaning properties, and extensive studies have been carried out to further characterize the photocatalysis phenomena and expand its practical application [1]. Three crystallographic structures of anatase, rutile, and brookite exist; monolithic anatase or dual phases of anatase and rutile have been considered to provide better photocatalytic activity [2,3]. The effect of the phase on quantum efficiencies has been provided for the above explanation in relation to the recombination rate of electrons and holes [4,5]. According to thermodynamic calculation, rutile is stable as compared to anatase. However, anatase becomes more stable than rutile when the particle size is small, due to size dependence of thermodynamic stability [6]. In contrast, high crystallinity lowers the fraction of crystal defects acting as recombination sites [7–9], allowing the generated charges to diffuse to the crystallite surface without recombination. Further, a large surface area increases the active sites in contact with matter to be photocatalytically decomposed, which is beneficial for photocatalytic activity [10,11]. These crystallographic and microstructural characteristics depend on fabrication method, and they affect the photocatalytic performance of the oxide complicatedly.

An anodic oxidation method has been used to fabricate TiO_2 on the surface of titanium and its alloys [12–15]. This method has several advantages. First, it allows one to select the composition of electrolytes used for doping; this is beneficial for controlling the band gap structure of the oxide [16,17]. Second, anodic oxidation occurs in equilibrium based on the thermodynamic reaction [18] and provides adhesion strength at the interface [19], which enables the growth of stable oxide layers. Third, it yields a porous microstructure due to the competitive reaction between oxide formation and chemical dissolution of the oxide [20,21], and distinct structures with tubular pores could be obtained [22–24]. Finally, the process fundamentals have been established for coloring titanium and its alloys [25], which is advantageous for application convenience. The conversion potential in anodic oxidation can vary the microstructure and phase of the oxide. Raising the conversion potential promotes crystallization, and increases the thickness of the oxide. Further increase in the potential generates sparking due to electric arcs through dielectric breakdown and a porous structure appears [26]. Other electrochemical conditions such as anodization time, current density, and concentration of the electrolyte could affect the crystal structure and microstructure of the oxide, and vary the photocatalytic activities [27,28]. Diamanti and Pedeferri concluded that anatase is promoted either by an increase in current density or by a decrease

* Corresponding author. Tel.: +81 22 215 2117; fax: +81 22 215 2116.
E-mail address: masahasi@imr.tohoku.ac.jp (N. Masahashi).

0926-3373/$ – see front matter © 2009 Elsevier B.V. All rights reserved.
doi:10.1016/j.apcatb.2009.03.011

in sulphuric acid concentration, and that porous morphology is obtained when a potential higher than 100 V and current densities higher than 400 A/m^2 is applied [29].

The authors have investigated hydrophilicity of the anodic oxide in low-concentration sulfuric acid electrolyte, and concluded that the superhydrophilicity of the oxide is related to the formation of highly crystallized anatase TiO_2 and the best performance is obtained by increasing the conversion voltage during anodic oxidation or subsequent annealing [30]. Recently, the authors reported that the superhydrophilicity of rutile TiO_2, prepared by anodic oxidation in an electrolyte with a high concentration of sulfuric acid, could be achieved without UV illumination [31]. In this study, the photocatalytic characteristics of the oxide prepared by anodic oxidation in an electrolyte with a wide range of sulfuric acid concentrations were investigated. Using the results of the previous study, the effects of the crystallinity and constituent phase on the photocatalytic characteristics were investigated, and the predominant factor governing the photoactivity of the anodic oxide was discussed.

2. Experimental

A pure titanium plate (cp-Ti, grade I) with dimensions of 20 mm × 10 mm × 1 mm that was to be used as the anode was chemically polished using a 40 nm colloidal silica suspension and was thoroughly washed in ethanol by using an ultrasonic cleaner. A constant current of 50 mA/cm^2 was applied to the Ti plate in a sulfuric acid electrolyte ranging from 0.002 M to 1.6 M, and a Pt mesh electrode was used as the cathode. The anodic oxidation was controlled galvanostatically until the conversion voltage reached 210 V, and the time duration of oxidation was fixed at 0.5 h. The anodized oxide was rinsed with distilled water and dried at room temperature, following by annealing at 723 K for 5 h in air. The crystallographic structure of the anodized oxide was determined by X-ray diffraction (XRD, PANalytical X'Pert diffractometer) with Cu-K_α radiation (0.15406 nm), a scan rate of 1°/min, a sample with a thin-film geometry arrangement at 0.5° glancing angle, and a rotating detector. Microstructure observations were conducted with field emission scanning electron microscopy (FESEM) using FEI XL-30FEG at an operating voltage of 3–15 kV and transmission electron microscopy (TEM) observations using JEOL JEM2000FX at an operating voltage of 200 kV. A TEM cross-sectional specimen of the oxide was prepared by a focused ion beam (FEI Quant D 200) at a voltage of 30 kV. Surface roughness and surface area were measured using a laser microscope with a wavelength of 408 nm (Keyence VK-9710). X-ray photoelectron spectroscopy (XPS) measurements were conducted with an electron spectrometer (ESCA1600, Ulvac-Phi) equipped with monochromated Al-K_α radiation.

The photocatalytic activity under UV light illumination was evaluated using methylene blue (MB) bleaching tests, wherein anodized oxide was placed in an optical quartz cell containing 2 ml of 25 mg/L MB aqueous solution until the MB concentration becomes constant to avoid the effect of the MB adsorption on the photocatalytic activities. A UV lamp (Ultra-Violet Product, 6 W), which provides UV light in the range of 340–400 nm with the central wavelength at 365 nm, was used with a filter to cut off the visible light. This could eliminate the effect of self-sensitization of MB because the overlap of the wavelength does not occur between MB absorption band and illuminated light. The intensity of the radiated light was 1.5 mW/cm^2 at the surface of the cell. The MB bleaching was evaluated by measuring the absorbance of MB at 664 nm using a UV–vis spectrophotometer (Jasco V-550) after UV illumination. MB solutions without photocatalysts were also illuminated in the same manner, and the absorbance at 664 nm was used as a blank value in calculations for the MB bleaching test. Further, the bleaching test was repeated in order to investigate the durability of the photocatalytic activity.

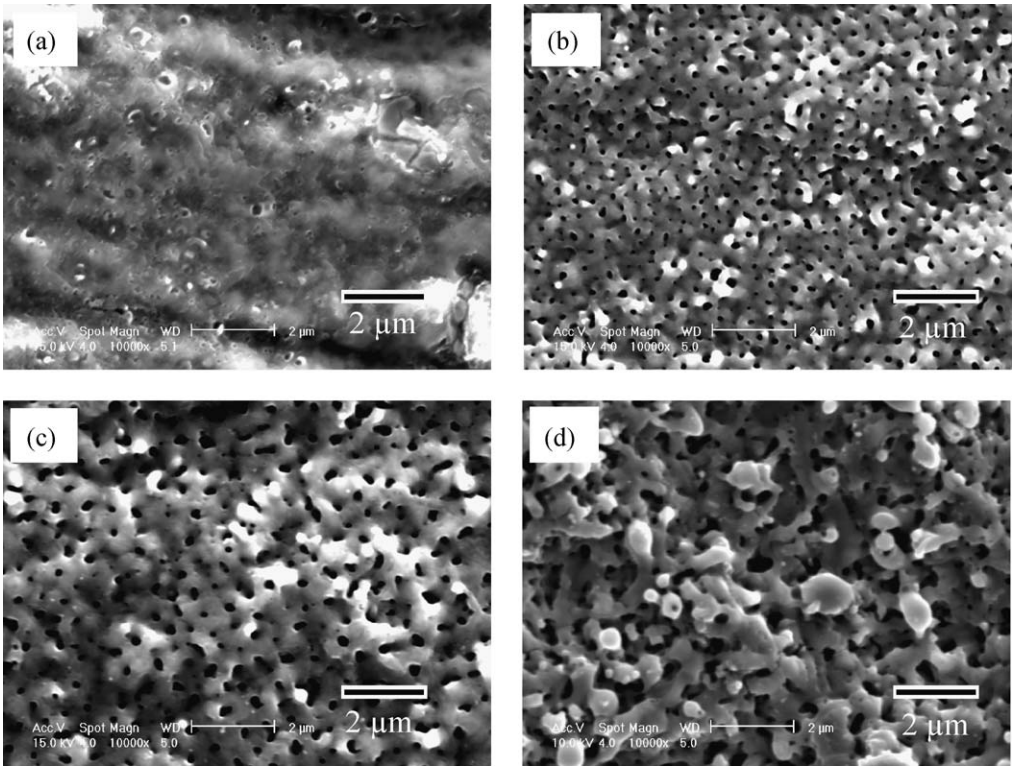

Fig. 1. FESEM microstructures of the oxides anodized in an electrolyte with a sulfuric acid concentration of 0.002 M (a), 0.1 M (b), 0.2 M (c) and 1.2 M (d).

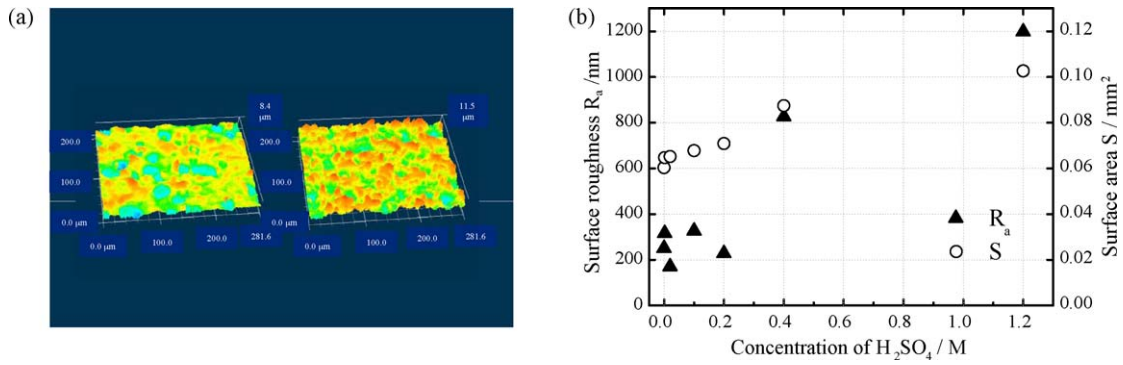

Fig. 2. The laser microscope images of the anodic oxide prepared in 0.4 M (left) and 1.2 M (right) sulfuric acid (a) and plots of the surface area (S) and the average roughness (R_a) of the anodic oxide against the sulfuric acid concentration in the electrolyte (b).

3. Results

3.1. Microstructures

Fig. 1 shows the microstructures of the annealed oxides anodized in an electrolyte of a sulfuric acid concentration of 0.002 M (a), 0.1 M (b), 0.2 M (c), and 1.2 M (d). When the sulfuric acid concentration is 0.002 M (a), glassy anodized oxide with submicron sized pores is observed. The pores are distributed inhomogeneously in shape and size, and their frequency is quite low. When the sulfuric acid concentration is 0.1 M (b), round-shaped pores appear homogeneously in the oxide, followed by growth of the pores with an increase of the sulfuric acid concentration of 0.2 M (c). Further increase in the concentration of sulfuric acid of 1.2 M (d) promotes a coalescence of each pore. The average pore size varies from approximately 170 nm to 950 nm, with the concentration of sulfuric acid. Distinct microcracks are not observed in the as-anodized and annealed oxides, regardless of the concentration of sulfuric acid, which is different from the oxides anodized in an electrolyte of a low concentration of sulfuric acid [30]. Fig. 2(a) shows the laser microscope images of the anodic oxide prepared in 0.4 M (left) and 1.2 M (right) sulfuric acid, revealing that the surface roughness of the oxide prepared in 1.2 M sulfuric acid is higher than that prepared in 0.4 M sulfuric acid. The surface area (S) and the average roughness (R_a) of the anodic oxide are plotted against the sulfuric acid concentration in the electrolyte (Fig. 2(b)). It shows that both the surface area and roughness increase with an increase of the sulfuric acid concentration in the electrolyte.

Fig. 3 shows the cross-sectional TEM images of as-anodized (a) and annealed (b) oxides prepared in an electrolyte with a sulfuric acid concentration of 1.2 M. It reveals that the thickness of the oxides are approximately 7 μm, irrespective of annealing, which is larger than that of the oxide anodized in the electrolyte with a sulfuric acid concentration of 0.002 M (approximately 0.3 μm) [30]. A thin layer on the titanium substrate with a thickness of approximately 200 nm is observed in both the as-anodized and annealed oxides. The inserted bottom-left and top-middle diffraction patterns are obtained from the areas indicated by circles (A) and (B), respectively; the area circled (A) and circled (B) show the anatase and rutile form, respectively. The grains in a microstructure possess specific orientations from the diffraction patterns, which is different from the as-anodized oxide prepared in an electrolyte with a sulfuric acid concentration of 0.002 M. Further, the grain size of the oxides is relatively large as compared to that of the oxide anodized in an electrolyte with a sulfuric acid concentration of 0.002 M [30].

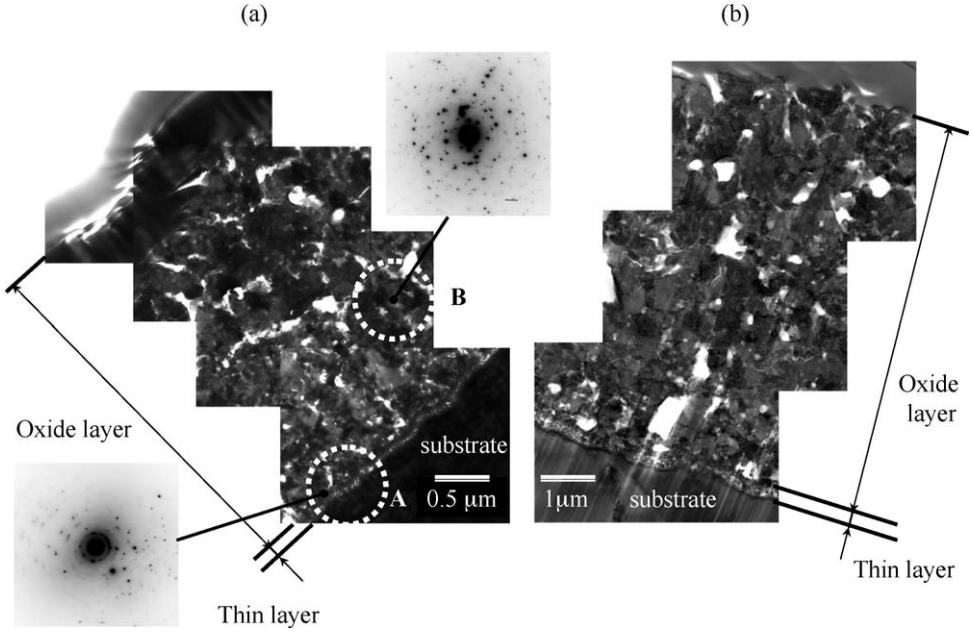

Fig. 3. Cross-sectional TEM micrographs of the as-anodized (a) and annealed (b) oxides anodized in an electrolyte with a sulfuric acid concentration of 1.2 M. The inserted bottom-left and top-middle diffraction patterns in (a) are obtained from the areas indicated by circles (A) and (B), respectively.

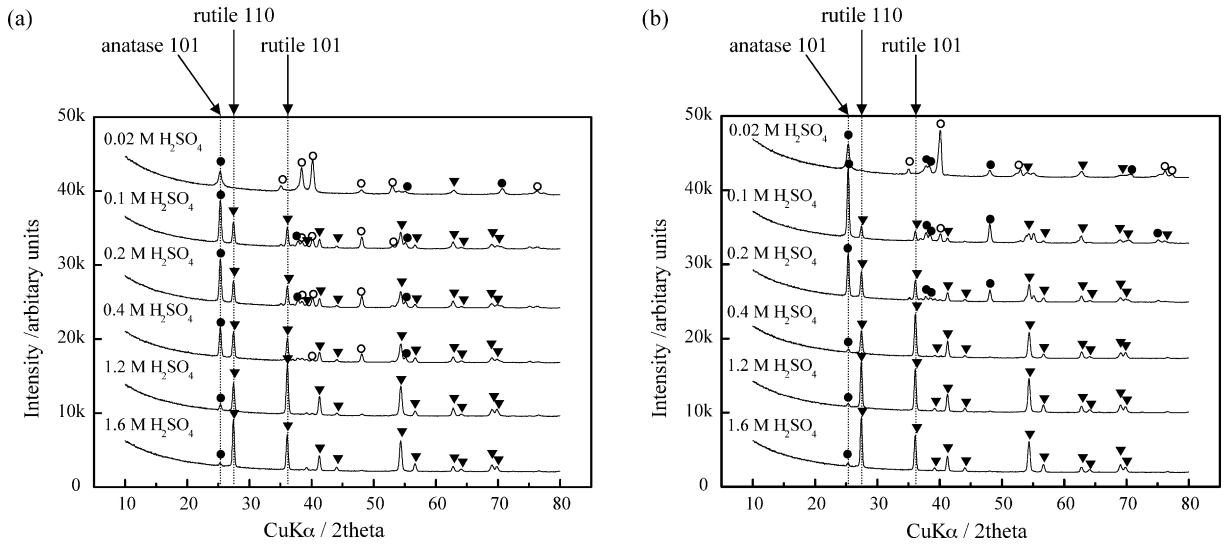

Fig. 4. XRD profiles of the as-anodized (a) and annealed (b) oxides anodized in an electrolyte with a sulfuric acid concentration of 0.02 M, 0.1 M, 0.2 M, 0.4 M, 1.2 M and 1.6 M; (●) anatase, (▼) rutile, (○) Ti.

3.2. Crystal structure

Fig. 4 shows the XRD profiles of as-anodized (a) and annealed (b) oxides prepared in an electrolyte with a sulfuric acid concentration of 0.02 M, 0.1 M, 0.2 M, 0.4 M, 1.2 M, and 1.6 M. The peak intensity of the substrate hcp-Ti (1 0 1) ($2\theta = 40.1^\circ$) decreases with an increase in the sulfuric acid concentration, indicating that the thickness of the oxide layer increases with the sulfuric acid concentration. The predominant oxide phase converted from anatase to rutile at 0.4 M of sulfuric acid in the electrolyte. The intensity of anatase (1 0 1) ($2\theta = 25.4^\circ$) increases with annealing, and the oxide anodized in 0.2 M sulfuric acid exhibits the highest intensity among the investigated oxides. In contrast, the major peak of rutile varied depending on the concentration of sulfuric acid. When the sulfuric acid concentration is less than 0.4 M, (1 0 1) ($2\theta = 36.1^\circ$) is the main peak. However, the intensity of (1 0 1) decreases with an increase in the sulfuric acid concentration and that of (1 1 0) ($2\theta = 27.4^\circ$) increases, suggesting that a different type of preferential orientation presents depending on the sulfuric acid concentration in the electrolyte. Several empirical equations were proposed to estimate the fraction of the constituent phase between rutile and anatase [32–34], while no distinct difference was found between them. Fig. 5 shows the result calculated by Eq. (1) [34].

$$f_{\text{rutile}} = \frac{0.679 I_{\text{rutile}}}{I_{\text{rutile}} + I_{\text{anatase}}} + 0.312\left(\frac{I_{\text{rutile}}}{I_{\text{rutile}} + I_{\text{anatase}}}\right)^2 \quad (1)$$

where I_{anatase} and I_{rutile} are the peak area of the main anatase and rutile reflections, respectively. It shows that the fraction of rutile increases with an increase in the sulfuric acid concentration in the electrolyte, irrespective of annealing, implying that the rutile form is stabilized with an increase in the sulfuric acid.

The crystallite size (L) and inhomogeneous lattice strain (ε) in the oxide were calculated from the full width at half maximum (FWHM) of the oxide peak by using Hall's Eq. (2).

$$\beta\cos\theta = K\frac{\lambda}{L} + 2\varepsilon\sin\theta \quad (2)$$

where L is expressed in nm, λ is the X-ray wavelength, β is the full width at half maximum of the signal in radians, K is the shape factor of 0.89, assuming that the crystallite is sphere, ε is lattice strain, and θ is the Bragg angle. In order to precisely calculate these parameters, XRD measurements were conducted at a scan rate of 0.02°/min. The parameters L and ε are plotted against the sulfuric acid concentration in Fig. 6(a) and (b), respectively. In Fig. 6, the parameters of the monolithic rutile TiO_2 powders with particle sizes of 1–2 μm (99.9%, Soekawa Chemical Co. Ltd., Japan) was plotted to compare with those of the anodic oxide. Fig. 6(a) shows that the crystallite size varied between 10 nm and 30 nm and decreased slightly with annealing. The crystallite size of anatase increases with the sulfuric acid concentration in the electrolyte, irrespective of annealing, and the as-anodized oxide exhibits a larger crystallite size than that of the annealed oxide. However, the crystallite size of rutile is approximately 30 nm, irrespective of the sulfuric acid concentration, and no explicit difference is found between the as-anodized and annealed oxide. Fig. 6(b) shows that the inhomogeneous lattice strain of the oxide is quite low or free (calculated as negative value) and annealing treatment further reduces the inhomogeneous strain.

3.3. XPS

Fig. 7 shows Ti 2p (a) and O 1s (b) XPS of the annealed oxides anodized in electrolytes of a sulfuric acid concentration of 0.1 M and 1.2 M, respectively. Two single peaks at approximately 465 eV

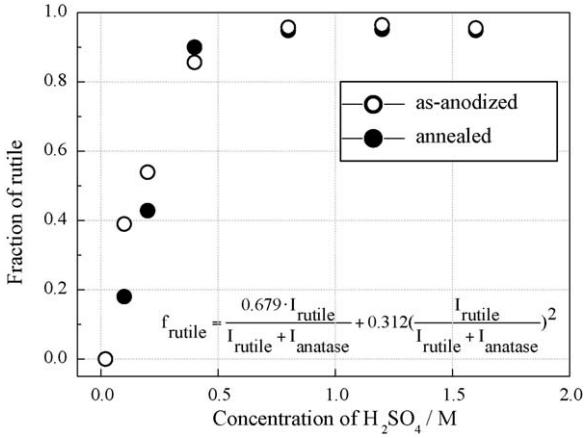

Fig. 5. Plots of the fraction of rutile in the as-anodized and annealed oxides calculated by the inserted equation against the sulfuric acid concentration in the electrolyte.

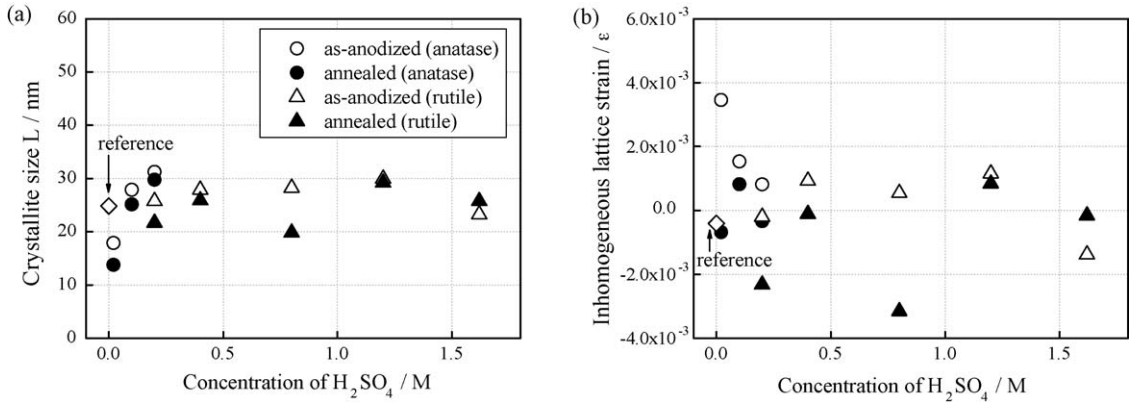

Fig. 6. Crystallite size (a) and inhomogeneous lattice strain (b) of the as-anodized and annealed oxides versus the sulfuric acid concentration in the electrolyte.

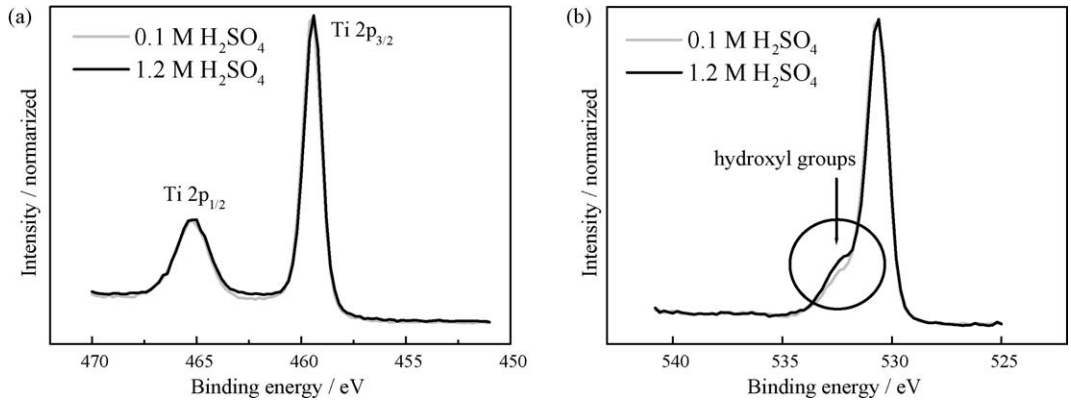

Fig. 7. Ti 2p (a) and O 1s (b) XPS spectrum of the oxides anodized in an electrolyte of a sulfuric acid concentration of 0.1 M and 1.2 M.

and 459 eV correspond to the Ti^{4+} $2p_{1/2}$ and $2p_{3/2}$ contributions of titanium dioxide. They have a symmetrical shape, indicating that reduced Ti^{3+} ions are not present in the oxides. The O 1 s XPS profiles have an asymmetrical shape accompanied with a shoulder band at approximately 532.4 eV on the higher binding energy side of the main peak. This shoulder peak has been observed in the previous study [30] and is ascribed to the adsorption of hydroxyl groups [35,36]. It should be noted that the intensity of the shoulder peak in the oxide anodized in the electrolyte with a sulfuric acid concentration of 1.2 M is higher than that in the electrolyte of a sulfuric acid concentration of 0.1 M. This suggests that the former anodic oxide could adsorb a large amount of hydroxyl groups as compared to the latter oxide.

3.4. Photocatalytic activities

The photocatalytic bleaching tests were conducted to evaluate the photocatalytic activities of the anodized photocatalysts. The experimental data was converted to a linear pattern using a pseudo-first-order kinetics model and results are shown in Fig. 8. Apparent reaction rate constants calculated by the slopes in Fig. 8 are plotted against the sulfuric acid concentration in the electrolyte

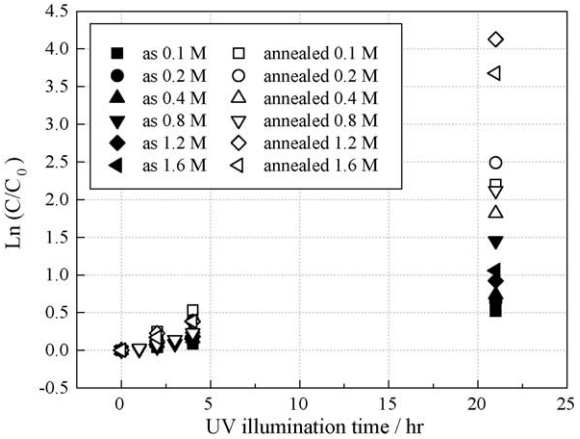

Fig. 8. The photocatalytic activities of the as-anodized and annealed oxides against UV light illumination time.

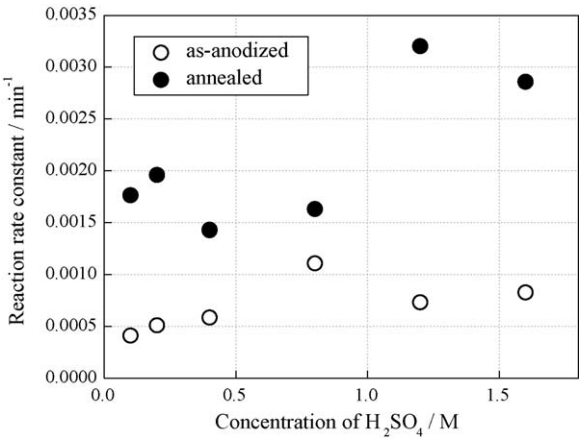

Fig. 9. Plots of the calculated reaction rate constant against the sulfuric acid concentration in the electrolyte.

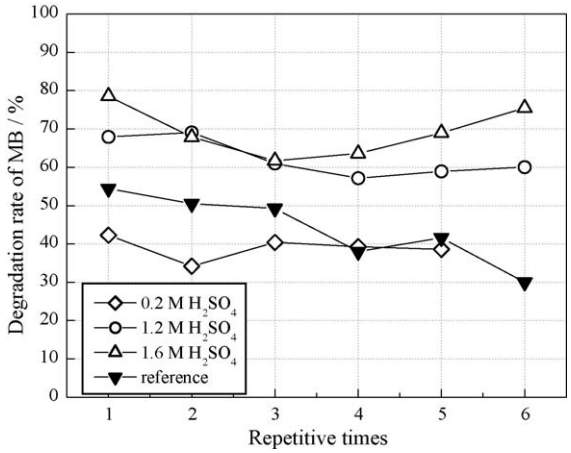

Fig. 10. Plots of the degradation rate of MB in the sequential bleaching test against the repetitive test times.

in Fig. 9. It is found that the annealed oxides show high activities as compared to as-anodized oxides, irrespective of the sulfuric acid concentration. In addition, the oxides anodized in the electrolyte with a high sulfuric acid concentration bleached MB with high efficiency. In order to explore the durability of the photocatalysts, the bleaching test was carried out repeatedly in 50 mg/L MB solution assuming practical use under further severe environments. The test was conducted sequentially without rinsing the oxide between the tests. The result was compared with anatase-structured TiO_2 fabricated by chemical vapor deposition (CVD) method as a reference (Fig. 9). The degradation rate of the reference gradually decreased with repetitive tests, whereas that in the rutile-structured oxide prepared by anodic oxidation in an electrolyte with a high concentration of sulfuric acid is not deficient as compared to the reference (Fig. 10).

4. Discussion

The photocatalytic activity of TiO_2 prepared by anodic oxidation varied with the sulfuric acid concentration in the electrolyte. The predominant phase in the anodic oxide changes from anatase to rutile with the sulfuric acid concentration, and rutile oxide exhibits better characteristics as compared to anatase oxide. It is generally accepted that the photocatalytic activity of anatase is superior to that of rutile. This superior photocatalytic activity can be ascribed to the fact that the Fermi level of anatase is higher than that of rutile by approximately 0.1 eV and that anatase has a lower rate of recombination due to the hole trapping effect [4]. It has been reported that a mixed phase of a large amount of anatase and residual rutile, such as commercial photocatalysis Degussa P25, has better photocatalytic activity than monolithic anatase and the rutile form [5,37]. This synergy effect of mixed phases has been explained by interfacial charge transfer between anatase and rutile [38–40], but there have been disputes about this explanation. In a photocatalytic reaction, the oxidation activity depends on the energy level of the valance band and the reduction activity depends on the energy level of the conduction band. Since MB decomposition progresses by oxidation reaction [41], the photocatalytic activity is affected by the energy level of the valence band. The energy edge of the valence band is comparable in both forms [42], implying that there should be no explicit difference in oxidation reaction between anatase and rutile. Thus, it is considered that the photocatalytic activity in the present study could be influenced by other factors such as the recombination rate of the electron and hole, the mobility of the electron and hole, and geometrical factors in the microstructure.

First, the crystallinity of the photocatalysis is considered. Crystallinity is defined as the degree of structural perfection and can be evaluated by inhomogeneous strain using XRD analysis. Low inhomogeneous strain reduces the number of crystal lattice defects like dislocation and vacancy, which become recombination centers of the photogenerated electron and hole. The structural analysis revealed that the inhomogeneous strain in the rutile-structured oxide is quite small, irrespective of the sulfuric acid concentration in the electrolyte, as shown in Fig. 6(b). Furthermore, the Ti 2p XPS spectra of the anodic oxides show a symmetrical profile (Fig. 7(a)), implying that reduced Ti^{3+} ions are not present in the oxides. These results imply the oxide contains a small number of recombination sites, which suggests that the rutile-structured anodic oxide has high crystallinity; as a result, the probability of the extinction of the photogenerated charges is quite low. Based on this discussion, the better photocatalytic activity of the annealed anodic oxides as compared to that of the as-anodized oxides (Fig. 9) could be explained by the variation of the lattice strain (Fig. 6(b)). However, the sulfuric acid concentration dependence of the photocatalysis activity cannot be explained only by crystallinity, because the photocatalytic activity increases with an increase in the sulfuric acid concentration of the electrolyte and high crystallinity is maintained irrespective of the sulfuric acid concentration. The second factor is the surface area of the oxide. The surface area of the present oxide increases with the sulfuric acid concentration in the electrolyte, as shown in Fig. 2(b). It should be noted that the surface area measured by the Brunauer–Emmett–Teller (BET) method [43] contains an area that is not illuminated by light because surface area is calculated by the quantity of absorbed gas to a specimen. In contrast, the present surface area is derived from the measurement of the surface geometry of the oxide using laser light illumination, wherein the surface area corresponds to the illuminated area. The porous microstructure is formed by the dissolution of oxides due to corrosive electrolytes with high sulfuric acid concentrations [29], and it appears in the oxides anodized in an electrolyte having a sulfuric acid concentration greater than 0.1 M. The sulfuric acid concentration dependence of the surface area is similar to that of photocatalytic activity. Consequently, the anodic oxides prepared in high concentration sulfuric acid electrolyte show a highly crystallized rutile form with nanosized pores and possess excellent photocatalytic activity due to their high surface area.

The present anodic photocatalysis is expected to be applicable in various fields such as the purification of organic pollutants in water due to the stability enduring the repeated utilization and biomaterials sterilizing chemical substances due to biocompatibility of titanium oxides. These practical applications are facilitated by the anodic oxidation method immobilizing TiO_2 stably on titanium and its alloys in arbitrary shape. The authors consider that the photocatalytic characteristics of the anodic oxides could be controlled by microstructural and crystallographic controlling through optimizing the electrochemical conditions to meet the expected properties for applications.

5. Conclusions

The photocatalytic activities of TiO_2 prepared by anodic oxidation are investigated in relation to the crystallinity and microstructure of the oxide. With an increase in the concentration of sulfuric acid in the electrolyte, the predominant phase converts from anatase to rutile and the surface area increases due to the appearance of nanosized pores in the oxide. The crystallite size of anatase increases with the sulfuric acid concentration and the as-anodized oxide exhibits larger crystallite size as compared to the annealed oxide, whereas that of rutile is essentially constant at approximately 30 nm, irrespective of the sulfuric acid concentra-

tion and annealing. The inhomogeneous lattice strain is quite small or close to zero in both forms. The photocatalytic activities evaluated by the methylene blue bleaching test shows that the photocatalytic activity is improved with an increase in the concentration of sulfuric acid and rutile exhibits better characteristics as compared to anatase. In conclusion, the photoactivity of rutile-structured TiO_2 anodized in a high sulfuric acid electrolyte exhibits the best performance among the investigated oxides, due to high crystallinity and high surface area.

Acknowledgements

The authors wish to thank Prof. Hanada for his valuable comments and encouragement to continue this study. We wish to acknowledge Ms. Y. Matsuda and Mr. S. Sugiyama from IMR, Tohoku University for the sample preparation, Mr. M. Yamane at Kitami Institute of Technology for XPS experiments and Mr. K. Hatanaka from Keyence Co., Ltd. for laser microscope observations. The authors are grateful to Dr. T. Moroishi, Mr. Y. Mitani, and Mr. R. Ozawa from Tig Co. Ltd. for helpful discussions. One of the authors (N.M.) received a Grant-in-Aid for Scientific Research (A) (No. 17206070) from the Ministry of Education, Culture, Sports, Science, and Technology, Japan.

References

[1] A. Fujishima, T.N. Rao, D.A. Tryk, J. Photochem. Photobiol. C 1 (2000) 1–21.
[2] M.R. Hoffmann, S.T. Martín, W. Choi, D.W. Bahnemann, Chem. Rev. 95 (1995) 69–96.
[3] R.I. Bickley, T.G. Carreno, J.S. Lees, L. Palmisano, R.J.D. Tilley, J. Solid State Chem. 92 (1991) 178–190.
[4] H.P. Maruska, A.K. Ghosh, Sol. Energy 20 (1978) 443–458.
[5] G. Riegel, J.R. Bolton, J. Phys. Chem. 99 (1995) 4215–4224.
[6] H. Zhang, J.F. Banfield, J. Mater. Chem. 8 (1998) 2073–2076.
[7] M. Inagaki, Y. Nakazawa, M. Hirano, Y. Kobayashi, M. Toyoda, Int. J. Inorg. Mater. 3 (2001) 809–811.
[8] A.G. Agrios, P. Pichat, J. Photochem. Photobiol. A 180 (2006) 130–135.
[9] G. Benko, B. Skarman, R. Wallenberg, A. Hagfeldt, V. Sundstrom, A.P. Yartsev, J. Phys. Chem. B 107 (2003) 1370–1375.
[10] O. Carp, C.L. Huisman, A. Reller, Prog. Solid State Chem. 32 (2004) 33–177.
[11] U. Černigoj, U.L. Štangar, P. Trebše, U.O. Krašovec, S. Gross, Thin Solid Films 495 (2006) 327–332.
[12] G.K. Mor, K. Shankar, M. Paulose, O.K. Varghese, C.A. Grimes, Nano Let. 6 (2006) 215–218.
[13] D. Velten, V. Biehl, F. Aubertin, B. Valeske, W. Possart, J. Breme, J. Biomed. Mater. Res. 59 (2002) 18–28.
[14] A.G. Mantzila, M.I. Prodromidis, Electrochim. Acta 51 (2006) 3537–3542.
[15] R. Palombari, M. Ranchella, C. Rol, G.V. Sebastiani, Solar Energy Mater. Solar Cells 71 (2002) 359–368.
[16] G.K. Mor, O.K. Varghese, M. Paulose, K. Shankar, C.A. Grimes, Solar Energy Mater. Solar Cells 90 (2006) 2011–2075.
[17] L. Lei, Y. Su, M. Zhou, X. Zhang, X. Chen, Mater. Res. Bull. 42 (2007) 2230–2236.
[18] A.L. Pergament, G.B. Stefanovich, Thin Solid Films 322 (1998) 33–36.
[19] Y. Park, K. Shin, H. Song, Appl. Surf. Sci. 253 (2007) 6013–6018.
[20] P. Kern, O. Zinger, J. Biomed. Mater. Res. Part A 80 (2007) 283–296.
[21] B. Yang, M. Uchida, H.-M. Kim, X. Zhang, T. Kokubo, Biomaterials 25 (2004) 1003–1010.
[22] V. Zwilling, M. Aucouturier, E. Darque-Ceretti, Electrochim. Acta 45 (1991) 921–929.
[23] D. Gong, C.A. Grimes, O.K. Varghese, W. Hu, R.S. Singh, Z. Chen, E.C. Dickey, J. Mater. Res. 16 (2001) 3331–3334.
[24] J.M. Macak, H. Tsuchiya, A. Ghicov, K. Yasuda, R. Hahn, S. Bauer, P. Schmuki, Curr. Opin. Solid State Mater., Sci. 11 (2007) 3–18.
[25] A.K. Sharma, Thin Solid Films 208 (1992) 48–54.
[26] D. Miller, S.M. Afara, M.J. Dignam, M. Moskovits, Chem. Phys. Lett. 100 (1983) 236–240.
[27] Y. Lai, L. Sun, Y. Chen, H. Zhuang, C. Lin, J.W. Chin, J. Electrochem. Soc. 153 (2006) D123–D127.
[28] K. Shankar, K.C. Tep, G.K. Mor, C.A. Grimes, J. Phys. D: Appl. Phys. 39 (2006) 2361–2366.
[29] M.V. Diamanti, M.P. Pedeferri, Corros. Sci. 49 (2007) 939–948.
[30] N. Masahashi, S. Semboshi, N. Ohtsu, M. Oku, Thin Solid Films 516 (2008) 7488–7496.
[31] N. Masahashi, Y. Mizukoshi, S. Semboshi, N. Ohtsu, Chem. Lett. 38 (2008) 1126–1127.
[32] D. Chen, D. Yang, Q. Wang, Z. Jiang, Ind. Eng. Chem. Res. 45 (2006) 4110–4116.
[33] R.A. Spurr, H. Myers, Anal. Chem. 29 (1957) 760–762.
[34] X. Fu, L.A. Clark, Q. Yang, M.A. Anderson, Environ. Sci. Technol. 30 (1996) 647–653.
[35] P.A. Thiel, T.E. Madey, Surf. Sci. Rep. 7 (1987) 211–385.
[36] L.Q. Wang, D.R. Baer, M.H. Engelhard, A.N. Shultz, Surf. Sci. 344 (1995) 237–250.
[37] T. Ohno, K. Sarukawa, K. Tokieda, M. Matsumura, J. Catal. 203 (2001) 82–86.
[38] R.I. Bickley, T. Gonzalez-Carreno, J.S. Lees, L. Palmisano, R.J.D. Tilley, J. Solid State Chem. 92 (1991) 178–190.
[39] D.C. Hurum, A.G. Agrios, K.A. Gray, J. Phys. Chem. B 107 (2003) 4545–4549.
[40] H. Nakajima, T. Mori, Q. Shen, T. Toyoda, Chem. Phys. Lett. 409 (2005) 81–84.
[41] T. Zhang, T. Oyama, A. Aoshimaa, H. Hidaka, J. Zhao, N. Serpone, J. Photochem. Photobiol., A 140 (2001) 163–172.
[42] K.M. Schindler, M. Kunst, J. Phys. Chem. 94 (1990) 8222–8226.
[43] S. Brunauer, P.H. Emmett, E.E. Teller, J. Am. Chem. Soc. 60 (1938) 309–319.